Zoology 119 (2016) 182–195

Contents lists available at ScienceDirect

Zoology

journal homepage: www.elsevier.com/locate/zool

Three-dimensional analysis of scale morphology in bluegill sunfish, *Lepomis macrochirus*

Dylan K. Wainwright*, George V. Lauder

Museum of Comparative Zoology, Harvard University, 26 Oxford Street, Cambridge, MA 02138, USA

ARTICLE INFO

Article history:
Received 9 September 2015
Received in revised form 18 January 2016
Accepted 29 February 2016
Available online 5 March 2016

Keywords:
Fish locomotion
Locomotor performance
Scale morphology
Scale surface structure

ABSTRACT

Fish scales are morphologically diverse among species, within species, and on individuals. Scales of bony fishes are often categorized into three main types: cycloid scales have smooth edges; spinoid scales have spines protruding from the body of the scale; ctenoid scales have interdigitating spines protruding from the posterior margin of the scale. For this study, we used two- and three-dimensional (2D and 3D) visualization techniques to investigate scale morphology of bluegill sunfish (*Lepomis macrochirus*) on different regions of the body. Micro-CT scanning was used to visualize individual scales taken from different regions, and a new technique called GelSight was used to rapidly measure the 3D surface structure and elevation profiles of in situ scale patches from different regions. We used these data to compare the surface morphology of scales from different regions, using morphological measurements and surface metrology metrics to develop a set of shape variables. We performed a discriminant function analysis to show that bluegill scales differ across the body – scales are cycloid on the opercle but ctenoid on the rest of the body, and the proportion of ctenii coverage increases ventrally on the fish. Scales on the opercle and just below the anterior spinous dorsal fin were smaller in height, length, and thickness than scales elsewhere on the body. Surface roughness did not appear to differ over the body of the fish, although scales at the start of the caudal peduncle had higher skew values than other scales, indicating they have a surface that contains more peaks than valleys. Scale shape also differs along the body, with scales near the base of the tail having a more elongated shape. This study adds to our knowledge of scale structure and diversity in fishes, and the 3D measurement of scale surface structure provides the basis for future testing of functional hypotheses relating scale morphology to locomotor performance.

© 2016 Elsevier GmbH. All rights reserved.

1. Introduction

Most bony fishes are covered in ossified plates called scales, which exhibit a broad range of morphological diversity. The scales typical of extant bowfins and teleosts consist of an acellular bone layer that covers a plate of haphazardly arrayed collagen fibers (Grande and Bemis, 1998; Sire and Akimenko, 2004). These scales are then arranged in imbricating patterns where a given scale overlaps with many others but remains uncovered posteriorly. This uncovered area is known as the posterior field, and its morphology has been used to categorize and describe fish scales for centuries (Agassiz, 1833). Elasmoid scales of teleosts are also organized into different types depending on their posterior field morphology: cycloid, ctenoid, crenate and spinoid (Roberts, 1993). Cycloid scales have a smooth posterior edge without any spines. Ctenoid scales have a posterior edge that is at least partly made of small, interlocking, tooth-like structures called ctenii (singular, ctenus) that form as separate ossifications and create a spiny posterior edge. Crenate scales are less common and have extra growths at the posterior margin that extend in flattened, finger-like projections. Finally, spinoid scales have spines on the posterior field that are not made of interlocking ctenii. Instead, their spines are part of the main body of the scale.

Although features of these basic scale types have been useful in studies of fish taxonomy (Cockerell, 1911; Lagler, 1947; Batts, 1964; Daniels, 1996; Grande and Bemis, 1998), there is relatively little work quantifying the pattern of scale variation within individuals (however, see Suzuki, 1971; Jawad, 2005; Esmaeili et al., 2007; Dapar et al., 2012). Further, the three-dimensional (3D) structure of scales is not well understood but is critical to the construction of hypotheses regarding the mechanical and hydrodynamic function

* Corresponding author.
E-mail addresses: dylanwainwright@fas.harvard.edu, dylan.wainwright@gmail.com (D.K. Wainwright).

http://dx.doi.org/10.1016/j.zool.2016.02.006
0944-2006/© 2016 Elsevier GmbH. All rights reserved.

of fish surface ornamentation. Some previous work has investigated scale-like armor and scale material properties of fishes (Vernerey and Barthelat, 2010; Yang et al., 2012; Zhu et al., 2012; Chintapalli et al., 2014), but there are few investigations on the hydrodynamic effects of scales. These previous hydrodynamic analyses have been conducted using rigid, non-moving models which do not reflect the pattern of oscillatory body bending that occurs during fish swimming (Burdak, 1986; Sagong et al., 2008). To investigate potential hydrodynamic effects of scale morphology on undulatory locomotion, we need to first understand scale surface morphology in three dimensions. To date, few studies have even quantified the morphology of teleost scales, and none have done so using the topography of in situ imbricating fish scales. We know of only two studies that examine the surface topography of teleost scales – and only one of these studies shows data on the elevation of scale surface features, and then only for a few individual scales (Sudo et al., 2002; Sagong et al., 2008). Understanding the 3D topography of scale surfaces is ultimately important to understanding the 3D hydrodynamic interactions happening along the body of fish, therefore scale morphology must be understood before hydrodynamic hypotheses for scale function can be developed.

The goals of the present study are to qualitatively and quantitatively describe the scale morphology of a focal species, the bluegill sunfish (*Lepomis macrochirus*), while also exploring a new surface imaging technique that allows measurement of the elevation of scale surface features. In this study, we were able to determine how the 3D structure of bluegill scales varies over different regions of the body, while also quantifying the 3D morphology of both scaled surfaces and single whole scales. Our initial hypothesis was simple: we expected scales to differ across the body of bluegill in both shape and surface structure, in part due to adaptation to differing amplitude of motion exhibited along the body during undulatory propulsion (Jayne et al., 1996; Drucker and Lauder, 2000; Standen and Lauder, 2005). Specifically, we used a novel system called GelSight (GelSight Inc., Waltham, MA, USA) to image the surface topography of scale patches from six regions of the body. This technique allowed us to measure scale shape and surface elevation, and to calculate surface metrics to describe the fish surface on regions of scales in situ. We also used computed tomography (CT) scanning to image individual whole scales from the same six patches to obtain more traditional measurements of size and shape of isolated scales.

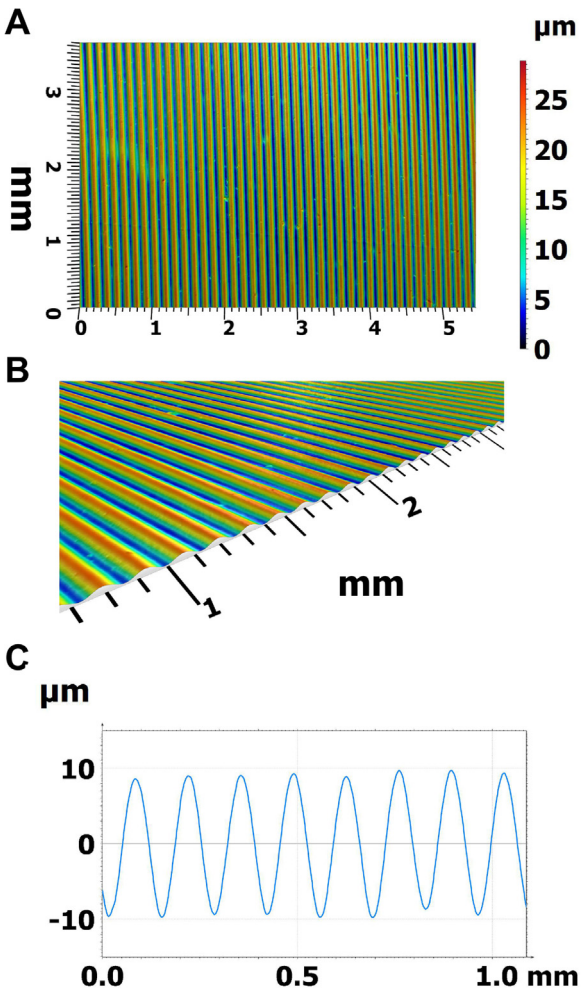

Fig. 1. GelSight was performed on a standard calibration surface with a sinusoidal pattern of known dimensions (see Section 2.2). (A) The sinusoid surface with peak-to-peak amplitude of 19 μm is displayed with a scale bar. (B) Also shown is an oblique view of the surface imaged with GelSight. (C) A profile of the surface is shown, where peak amplitude is within 2% of the expected 19 μm and the wavelength is not significantly different from the expected 135 μm.

2. Materials and methods

2.1. Study animals

Bluegill (*Lepomis macrochirus*) were used for the present study due to the considerable body of previous data on body shape, swimming mechanics, hydrodynamics, and energetics in this species (Kendall et al., 2007; Flammang and Lauder, 2008; Ellerby and Gerry, 2011; Flammang et al., 2011; Gerry et al., 2011). *L. macrochirus* is a freshwater fish found throughout North America in a wide range of habitats, but it does best in areas of slow flow. Specimens were taken from the Harvard Museum of Comparative Zoology's (MCZ) Ichthyology Collection. Three individuals of the same size class and in good condition were chosen for study from MCZ 101480 (Yawgoo Millpond, Slocum, RI, USA; April 8th, 1993; 10.84–11.83 cm standard length). Specimens were initially fixed in 3.7% formalin and then preserved in 70% ethanol after fixation. It is important that the fish be from the same population because intraspecific differences in scale morphology among populations have been documented in other species (Richards and Esteves, 1997). The three fish used had standard lengths of 11.31 cm, 10.84 cm, and 11.83 cm giving a mean standard length of 11.32 cm and a standard deviation of 0.49 cm.

2.2. GelSight imaging and analysis

GelSight is a new surface imaging technique that was used for the present study. It has been used in robotics to recognize surface textures and pressures (Li and Adelson, 2013; Li et al., 2014), but has never before been used for biological surface analysis. GelSight is a two-component system consisting of a camera and a piece of elastomer gel (Johnson and Adelson, 2009; Johnson et al., 2011). Proprietary gels (http://www.gelsight.com/) are made where one side is coated in reflective paint. The reflective side is pressed into the object of interest so the gel conforms to the surface of the object. An array of six LED lights allows illumination of the gel from different angles, and six photographs are taken using different angles of illumination (Fig. 1). Once the system is calibrated using a surface with known geometry, the GelSight software then processes these photographs into a 3D surface where each pixel is a 3D point. This system is non-damaging and can be performed on optically clear and wet material, allowing us to sample non-destructively without sample preparation, even on clear scales. This is in contrast to

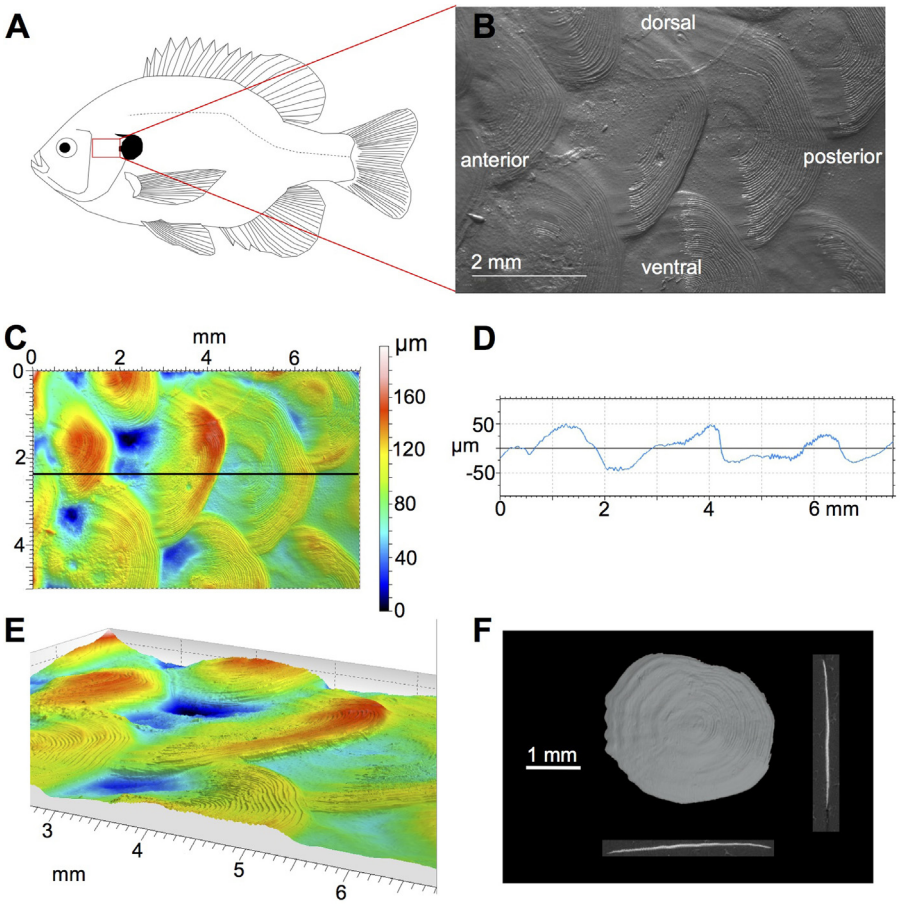

Fig. 2. Scales from the opercle region of *Lepomis macrochirus*. (A) Scales were imaged on the gill cover (opercle) of bluegill sunfish. (B) Grayscale image of the opercular scale surface – all panels show scales in this anatomical position. Note that scales are cycloid (without ctenii) and have small concentric circuli. (C) We show the surface in three-dimensions as a colored elevation map with a scale bar. (D) A profile line graph along the black reference line from C shows the topography of the surface – the plateaus and hills are the posterior fields, which are between 1.5–2.2 mm long with peak to valley heights of 50–100 μm. The small oscillations on the plateaus are caused by the circuli. (E) We also show an oblique view of the surface with elevation visually exaggerated by 10% to illustrate the 3D nature of these data. (F) Whole scales were imaged with μCT and an opercle scale is displayed with sagittal and transverse cross-sections. The scales of the opercle are oval in general shape and lack radii, although radii-like ridges are visible in the anterior region of the scales.

other surface imaging techniques that require sample preparation, especially on wet or clear material.

We used three bluegill specimens for GelSight, and on each specimen we investigated the same six body regions (with the name we have given each region in parentheses): (i) the operculum or gill-cover of the fish (opercle), (ii) between the spinous dorsal fin and the lateral line (dorsal), (iii) between the lateral line and the pectoral fin (central), (iv) between the pectoral fin and the underside of the body (ventral), (v) below the lateral line at the anterior caudal peduncle (peduncle), and (vi) below the lateral line on or near the hypural plate, but not on the caudal fin rays (tail). We always imaged the left side of the fish. Panel A in each of Figs. 2–7 shows the location of the sites sampled (opercle, dorsal, central, ventral, peduncle, and tail). We did not attempt to image the exact same scales on different fish, but limited our sampling to these small regions and used patches of scales that appeared undamaged. Scale surfaces were lightly brushed with a paintbrush to clean them of debris before imaging. We used a zoom lens to take images measuring 7.52 mm by 5.01 mm with a point density of 5202 by 3465, giving pixel resolution of 1.45 μm in the plane of the scan. One scan at each of the six regions was taken on each of the three fish.

To demonstrate the validity of this approach, we also used GelSight to image a sinusoidal surface standard with known dimensions (Fig. 1). This surface is made of symmetrical sinusoid riblets of amplitude 19 μm and wavelength 135 μm. This roughness standard is #525E (Rubert & Co. Ltd, Cheadle, UK), and represents a calibrated ISO industry-standard for surface metrology. GelSight imaging provided values that are very close to the specified dimensions; after measuring values at eight peaks, we found a mean peak-to-peak amplitude of 18.65 μm, reflecting a small but significant difference of 0.35 μm, or about 1.8% of 19 μm (t-test, $t = -2.579$, df = 7, $p = 0.0365$). We found no statistical difference in wavelength from the manufacturer's specified 135 μm (t-test, mean = 134.8 μm, $t = -0.378$, df = 7, $p = 0.72$). These values show that GelSight is a valid method for recovering surface geometry down to the micron scale.

GelSight scans were analyzed individually using TalyMap Platinum v5.1 (Digital Surf, Besançon, France), which is a surface analysis software package. Each surface was smoothed using TalyMap's "remove form" function. This corrects the surface to remove any large-scale curvature, while keeping the surface texture intact – an important correction to allow comparison of surface structure among samples. We then used TalyMap to generate values for 30 different surface metrology variables. We decreased and refined the number of metrology parameters during our statistical analysis, as explained in Section 3.2.

GelSight also creates 2D greyscale images of the regions that were scanned. We used these images to measure 2D morphological features of each scanned region in ImageJ v1.45s (Rasband, 1997–2015). We measured six variables on three posterior fields

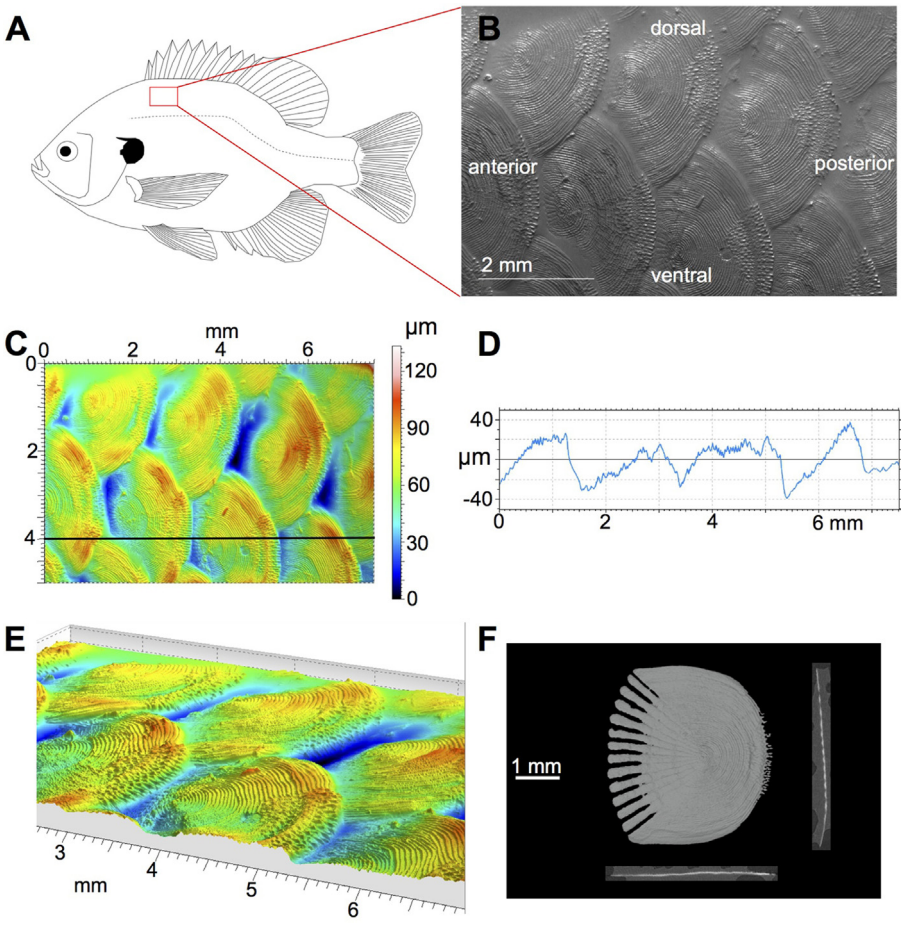

Fig. 3. Scales from the dorsal region of *Lepomis macrochirus*. (A) Scales were imaged on the dorsal region of fish, in the area between the first dorsal spines, and the lateral line. (B) Grayscale image of the opercular scale surface – all panels show scales in this anatomical position. (C) Scales in this region are ctenoid. We show the surface in three-dimensions as a colored height map with a scale bar. (D) The reference line in C is graphed as a profile line with zero as the average elevation of the surface. Hills correspond to posterior fields, which are around 2 mm long with peak to valley heights of 50–80 μm. (E) We also show an oblique view of the surface with elevation visually exaggerated by 10% to illustrate the 3D nature of these data. (F) We imaged individual scales with μCT, allowing us to display cross sections of scales as well as their three-dimensional representations. Radii are present and widely spaced along the anterior scale margin, which is covered by more anterior scales and not visible in images B-E.

for each scan: (i) posterior field height (dorsoventral axis), (ii) posterior field length (anteroposterior axis), (iii) posterior field area, (iv) area covered in ctenii, (v) length of the posterior margin, and (vi) length of the posterior margin made of ctenii. However, three full posterior fields were not always visible in each scan, so instead measurements were taken over half of the posterior field and multiplied by two. The three values for each variable were averaged for the scan, and that average was then used in statistical analyses. In addition, we used the six measured variables to calculate three metrics of posterior field shape and morphology: posterior field aspect ratio, percent of posterior field ctenii coverage, and percent of the posterior margin made of ctenii. We calculated posterior field aspect ratio by dividing the posterior field height by the posterior field length measurements, meaning lower values correspond to a posterior field more stretched in the anteroposterior axis. We calculated percent of posterior field ctenii coverage by dividing the area of the posterior field covered with ctenii by the total area of the posterior field. We calculated the percent of the posterior margin made of ctenii by similarly dividing the length of the posterior margin made of ctenii by the entire length of the posterior margin. These nine variables, three of which were calculated from the other six, were combined with the 30 surface metrology variables in an analysis to decrease and refine the number of variables as explained in Section 3.2.

2.3. μCT imaging and analysis

CT-scans have advantages over traditional microscopy techniques because they allow for a reconstruction of 3D morphology and they separate hard tissue, supplying data on the density of the region of interest. For the present study, we made use of CT scans instead of microscopy to accurately measure the thickness of scales and show that scales can be imaged accurately using μCT.

After GelSight scanning, we removed individual scales from only the specimen measuring 11.31 cm in standard length. Scales were taken from all six regions of interest described in Section 2.2 (opercle, dorsal, central, ventral, peduncle, and tail). We used a SkyScan 1173 micro-CT scanner (Bruker microCT, Kontich, Belgium) at a resolution of 6.75 μm voxel size to create our computed tomography (CT) data. For all scans, we used a voltage of 40 mV and a current of 200 μA. We removed four scales from each region sampled (opercle, dorsal, central, ventral, peduncle, and tail) and scanned each region's scales together, but only analyzed three scales from each region. The extra scale allowed us to discard scales that were damaged or bent in preparation but went unnoticed until the scan. These scans were reconstructed as image stacks using the program NRecon v1.6.9 (Bruker microCT). We used Mimics v16.0.0.235 (Materialise, Leuven, Belgium) to resolve our image stacks into 3D models.

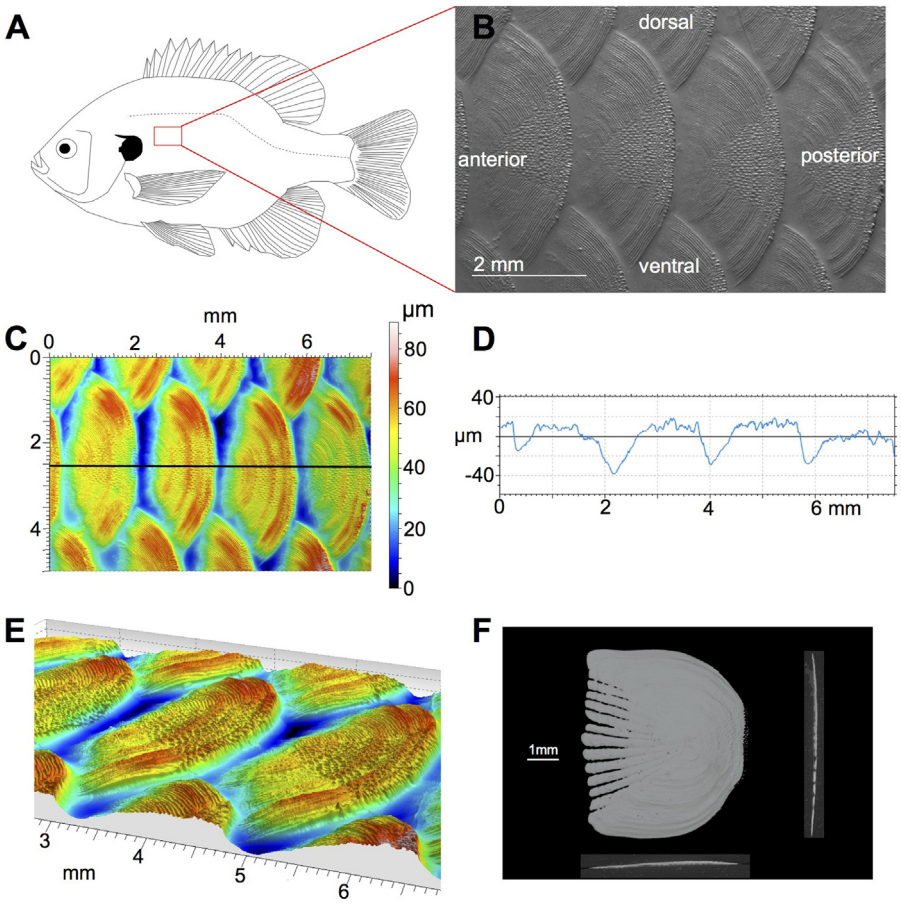

Fig. 4. Scales from the central region of *Lepomis macrochirus*. (A) Scales were imaged between the lateral line and pectoral fin in the area ventral to the spinous dorsal fin. (B) Grayscale image of the opercular scale surface – all panels show scales in this anatomical position. (C) Scales in this region are ctenoid. We show the surface in three-dimensions as a colored elevation map with a scale bar. (D) The black line in C is shown as a profile, where the mean height is zero. The posterior fields correspond to the plateaus in D and are approximately 1.9 mm long with deviations of 40–60 μm in elevation. Small deviations on the plateaus correspond to circuli and ctenii. (E) Three-dimensional data are shown at an oblique angle with a 10% height amplification – the scale bar from C still applies to E. (F) μCT scan of a single scale from this region with sagittal and transverse cross-sections that show small gaps between radii. Scale has a relatively blunt posterior margin.

Using the 3D models of the scales, we used Mimics to measure six variables for each of the three scales from each region: scale thickness, scale length, scale height, ctenii length, radii count, and scale aspect ratio. We measured scale thickness in the mediolateral axis at the approximate geometric center of the scale, scale length as the length in the anteroposterior axis at approximately 50% of its height, scale height in the dorsoventral axis at approximately 50% of its length, and ctenii length as the length of a single chosen ctenus. We also counted the number of radii present on each scale – radii are radially oriented thin regions or gaps (where ossification is reduced or lacking) in the bony scale matrix on the anterior portion of each scale (see panel F in Figs. 3–7). Scale aspect ratio was calculated by dividing scale height by scale length.

3. Results

3.1. Qualitative scale morphology

Figs. 2–7 present analyses of scales from the six different body surface regions we sampled in the following order: opercle, dorsal, central, ventral, peduncle, and tail. In all scales, growth rings (circuli) are visible on the posterior field. Radial gaps in the anterior field, called radii, are also evident in μCT images of single whole scales (panel F in Figs. 3–7).

Different regions of the body show clear differences in scale morphology, both in single whole scales and scaled surfaces. One of the most obvious differences is that scales on the opercle (Fig. 2) are cycloid with smooth posterior edges, while scales elsewhere on the body (Figs. 3–7) are ctenoid with small interlocking spines on the posterior field. Even on scales with ctenii, there are different proportions of ctenii coverage in different regions of the body – for example, dorsal scales (Fig. 3) have fewer ctenii than central scales (Fig. 4). Scales on the opercle (Fig. 2) also vary more in posterior field shape and whole scale shape than other regions.

There are also qualitative differences among the μCT-scanned whole scales (panel F in Figs. 2–7). Opercle scales are ellipsoid in shape, dorsal scales have more rounded corners, peduncle scales have flared anterior corners, and tail scales have a slightly pointed posterior edge. Also, radii in the anterior portion of bluegill scales differ among different regions. Notably, opercle scales have no radii (Fig. 2F), and dorsal scales have the widest radii, giving them the widest gaps in their anterior field (Fig. 3F).

Elevation profiles for each region are shown in panel D of Figs. 2–7. Note that each profile shows three to four posterior fields, each indicated by the larger plateaus in each graph. Posterior fields range in peak-to-valley heights from 35 μm to 125 μm: opercle posterior fields show peak-to-valley heights from 50 to 100 μm, dorsal from 40 to 80 μm, central from 35 to 80 μm, ventral from 40 to 70 μm, peduncle from 60 to 75 μm, and tail from 75 to 125 μm (panel D in Figs. 2–7). Color scale bars in panel C of Figs. 2–7 also show the elevation range across the entire surface.

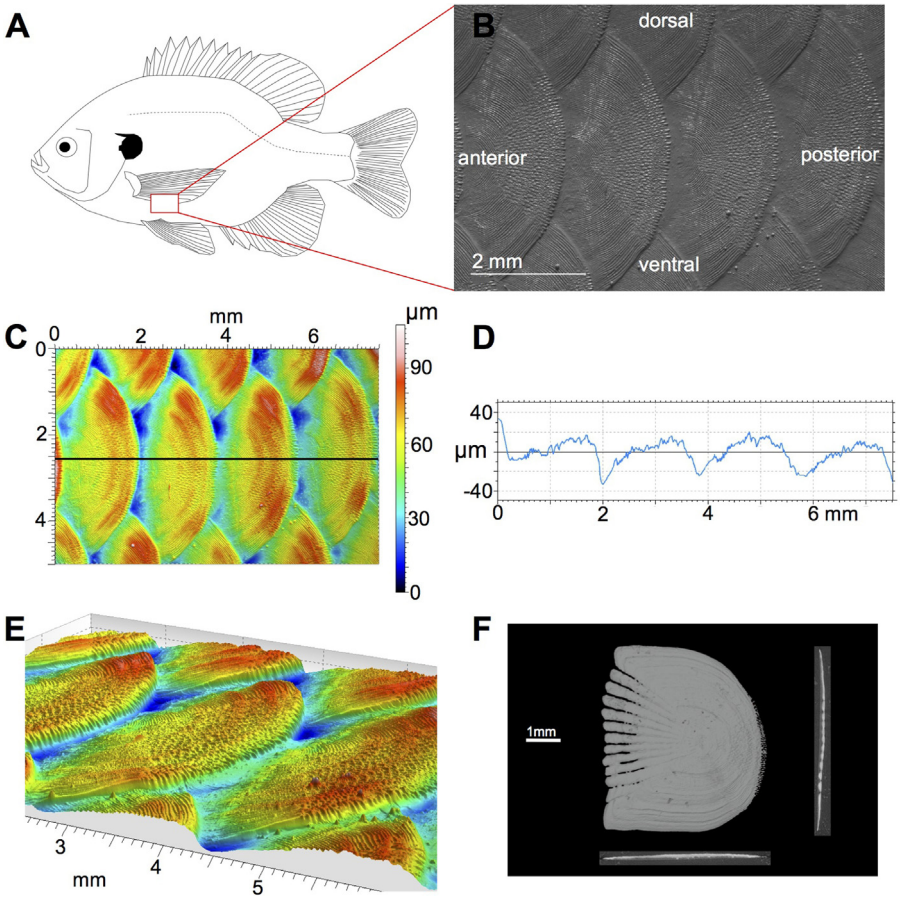

Fig. 5. Scales from the ventral region of *Lepomis macrochirus*. (A) Scales were imaged on the ventral surface of bluegill sunfish, between the pectoral fin and the pelvic fin. (B) Grayscale image of the scale surface – all panels show scales in this anatomical position. (C) Ventral scale surface in three-dimensions shown as a colored height map with a scale bar. (D) An elevation profile graph along the black line in C shows topography of the scaled surface – the hills are the posterior fields of scales, which are around 1.8 mm long with peak to valley heights of 30–50 μm. Oscillations in the height of the line in the plateau regions are caused by the circuli and ctenii. (E) An oblique view of the surface with elevation visually exaggerated by 10% to illustrate the 3D nature of these data. (F) Whole scales were imaged with μCT and a representative ventral scale is displayed, including sagittal and transverse cross-sections. Ventral scales have radii, ctenii, and a more rounded posterior edge. Radii are similar to those in central body scales.

3.2. GelSight results

Using GelSight we were able to measure 39 variables, which included 30 surface metrology variables and 9 parameters of size, shape, and ctenii coverage on posterior fields. Because of our large number of exploratory variables, we first reduced the number of variables for analyses, specifically to remove highly correlated variables. We used a correlation matrix to find variables that were the most positively or negatively correlated with one another. Because highly correlated variables show similar trends, we then removed variables until we had a set of only weakly correlated variables (correlation coefficients with an absolute value <0.82, although most are <0.6). This process left us with seven standard surface metrology variables: root-mean-square roughness, skew, kurtosis, texture direction, texture aspect ratio, mean hill area, and peak density, and two morphometric variables: posterior field aspect ratio, and percent of ctenii coverage. The variables that show significant trends are discussed below and incorporate aspects of 3D, 2D, and linear measurements. Although choosing one variable from a group of correlated ones can be arbitrary, we chose these variables for further analyses because they are both commonly used in surface metrology studies (Whitehouse, 1994) and more easily understood than other metrics.

With these nine variables, we used a MANOVA to test for differences among the six regions of the body. Differences among individuals are much smaller than the differences among scale regions (Fig. 8). The MANOVA showed a significant difference in scale surface structure among body regions: Wilks: $p = 0.0018$, Pillai: $p = 0.0027$. To display this result, we use a discriminant function analysis, which creates discriminant functions composed of the nine variables that best group the data by body region (Fig. 8A). Our first discriminant function explains over 75% of the variability between groups, while our second discriminant function explains nearly 14% (Fig. 8A). With MANOVA results indicating differences among scale patches from different regions of the body, we then ran post hoc ANOVAs on each variable to determine which were the ones contributing to differences among scale patches. Four variables showed significant trends: percent of ctenii coverage ($p = 0.0036$), aspect ratio ($p = 0.0057$), skew ($p = 0.035$), and texture direction ($p = 0.038$). A Tukey HSD test was then performed on each significant variable to see which specific regions of the fish differed with respect to each variable using a standard alpha level of 0.05. These results are presented graphically in Fig. 8B–E, with statistical groups shown by the grey and black lines at the top of each graph.

As seen in Fig. 8B, the percent of ctenii coverage shows two groups with much overlap; ctenii coverage on tail scales is greater than on opercle and dorsal scales, while ctenii coverage on ventral scales is greater than on opercle scales (Tukey HSD; tail–opercle: $p = 0.004$, tail–dorsal: $p = 0.026$, ventral–opercle: $p = 0.016$). In general, we observe more ctenii coverage as we move ventrally on the fish from dorsal to central and then ventral scales, and ctenii coverage is higher on scales from the posterior part of the fish on the

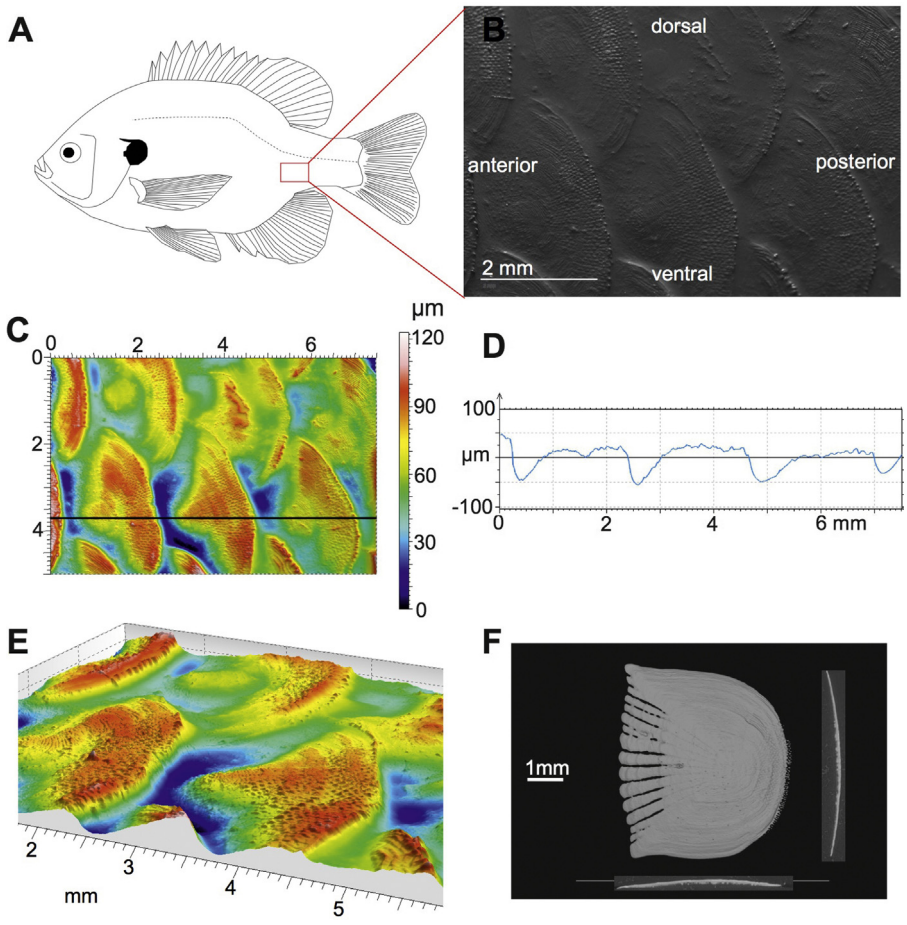

Fig. 6. Scales from the peduncle region of *Lepomis macrochirus*. (A) Scales were imaged between the lateral line and posterior base of the anal fin. (B) Grayscale image of the surface – all panels show scales in this anatomical position. (C) Ctenii are present and ctenii fields are triangular. Scale surface in three-dimensions as a colored elevation map with a scale bar. (D) An elevation profile graph along the black line in C shows topography. The plateaus are posterior fields – around 2.2 mm long and showing peak to valley heights of 60–80 µm. (E) Oblique view of this surface with elevation exaggerated by 10% to illustrate the 3D nature of these data. (F) µCT reconstruction of an anterior peduncle scale is displayed, including sagittal and transverse cross-sections. Peduncle scales show radii, ctenii, and have rounded posterior margins with flared dorsal and ventral edges. Radii nearest the lateral edges are not fully open.

peduncle and tail regions. Values fluctuate from around 10% ctenii coverage of the posterior field in the dorsal region to 35% in the tail region.

Fig. 8C shows the relationship between aspect ratio of the posterior field and region of the body. We find that posterior fields of opercle scales have a smaller aspect ratio than those on the central and ventral regions (Tukey HSD; opercle–central: $p = 0.0073$, opercle–ventral: $p = 0.0047$). Aspect ratio is lowest on the opercle region and increases from dorsal to central on the body of the fish.

Fig. 8D shows that skew is lower in the tail region than it is in the peduncle region (Tukey HSD, peduncle–tail: $p = 0.022$). Skew is a surface metrology metric where positive values indicate a predominance of peaks on the surface, whereas negative values indicate more valleys. The peduncle region is the only region with positive skews, although values for all regions of the bluegill are close to zero, indicating that surfaces contain equivalent peaks and valleys – evident from the profile lines given in panel D of Figs. 2–7.

Finally, in Fig. 8E we show the texture direction over different regions of the body. Texture direction is the direction of the primary pattern of a surface and is measured in degrees counterclockwise relative to the y-axis. A texture direction value of 90° means the prominent pattern of the surface would be arranged along the x-axis of the images (left to right in images presented). Although there are no differences between groups with a Tukey HSD test using a 0.05 alpha level, texture direction shows a significant overall effect, indicating that while texture differences among any pair of regions is small, significant variation still exists across all regions (considered together) in this metric.

3.3. µCT results

Measurements from µCT reconstructions include scale length, height, thickness, ctenii length, number of radii, and scale aspect ratio, and these data are shown in Fig. 9. Scale length is measured along the anteroposterior axis, scale height is measured along the dorsoventral axis, and scale thickness is measured in the mediolateral axis (for details see Section 2.3). MANOVA analysis shows a difference among scales from different body regions using these six variables (Wilks: $p < 0.001$, Pillai: $p < 0.001$).

Scales from different regions show differences in length (ANOVA, $p < 0.001$), although the pattern among regions is complex (Fig. 9A). Scales from the opercle are shorter in length than scales from the central, ventral, peduncle, and tail regions (Tukey HSD; opercle–central: $p < 0.001$, opercle–ventral: $p < 0.001$, opercle–peduncle: $p = 0.0073$, opercle–tail: $p = 0.0012$). Additionally, dorsal scales are shorter than scales from the central, ventral, and tail regions (Tukey HSD; dorsal–central: $p = 0.0067$, dorsal–ventral: $p = 0.017$, dorsal–tail: $p = 0.041$). Overall, scales are shorter on the opercle and dorsal regions (~4 mm) and longer on the rest of the body (~5 mm).

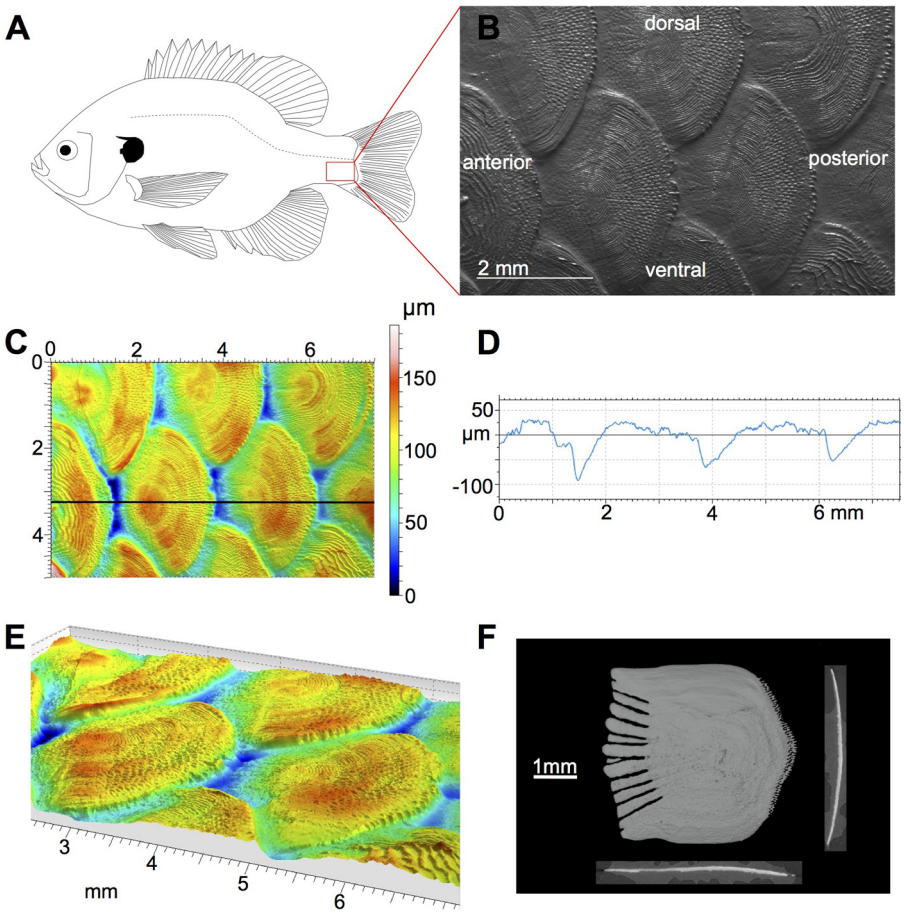

Fig. 7. Scales from the tail region of *Lepomis macrochirus*. (A) Scales were imaged above the hypural plate at the base of the tail, and below the lateral line. (B) Grayscale image of the surface – all panels show scales in this anatomical position. Ctenii present. Note the replacement scales with more distantly spaced circuli in the bottom right, top right, and left edges of the image. (C) The scale surface is shown in three-dimensions as a colored elevation map with a scale bar. (D) An elevation profile graph from the black line in C shows the topography of the scaled surface – the plateaus are the posterior fields, which are around 2.4 mm long and show vertical deviations of 80–120 μm. (E) Oblique view of the surface with elevation visually exaggerated by 10% to illustrate the 3D nature of these data. (F) Whole scales were imaged with μCT and a single tail scale is displayed, including sagittal and transverse cross-sections. Scales have dull-pointed posterior edges, straightened lateral edges, and slightly flared anterior margins. Radii nearest the lateral edges are not fully open.

Scales are also different in height (ANOVA, $p < 0.001$) as shown in Fig. 9B. Opercle scales are shorter in height compared to scales from the central, ventral, and peduncle regions (Tukey HSD; opercle–central: $p < 0.001$, opercle–ventral: $p = 0.0014$, opercle–peduncle: $p = 0.0026$). Similarly, dorsal scales are shorter than scales from the central, ventral, and peduncle regions (Tukey HSD; dorsal–central: $p = 0.0055$, dorsal–ventral: $p = 0.023$, dorsal-peduncle: $p = 0.045$). Tail scales are also shorter than central scales (Tukey HSD; tail–central: $p = 0.020$).

Fig. 9C shows that the thickness of scales is different on different regions of the fish (ANOVA, $p < 0.001$). Scales from the opercle region are thinner than scales from the central, ventral, and peduncle regions (Tukey HSD; opercle–central: $p = 0.0024$, opercle–ventral: $p = 0.025$, opercle–peduncle: $p = 0.013$). Moreover, scales from the dorsal region are thinner than scales of the central, ventral, peduncle, and tail regions (Tukey HSD; dorsal–central: $p < 0.001$, dorsal–ventral: $p = 0.0011$, dorsal–peduncle: $p < 0.001$, dorsal–tail: $p = 0.011$). Opercle and dorsal scales are thinnest, at about 65 μm, while central, ventral, and peduncle scales are much thicker, at around 110 μm.

Fig. 9D shows that length of ctenii is different among different regions on bluegill (ANOVA: $p < 0.001$). The only statistical difference here is that scales from the opercle region have no ctenii, in contrast to ctenii being present on all other scale regions (Tukey HSD: all pairwise comparisons between opercle and other regions $p < 0.001$). In the present study we have chosen to characterize the cycloid scales of the opercle as having ctenii of zero length, but an argument could be made for treating ctenii presence as a categorical variable. However, some research suggests that with growth of a fish, cycloid scales become ctenoid scales in some species, indicating that some cycloid and ctenoid scales are on the same ontogenetic spectrum of scale types (Burdak, 1986). It is possible that finer differences would be seen with a larger sample size. Dorsal, central, ventral, peduncle, and tail regions have ctenii about 110 μm long.

Fig. 9E shows that scale radius number differs among regions (ANOVA: $p < 0.001$). Opercle scales are different from other regions because they have either very few or no radii (Tukey HSD: all pairwise comparisons between opercle and other regions $p < 0.001$). The pairwise comparison between the counts of central versus peduncle radii is close to significance ($p = 0.081$) – indicating a larger sample size could reveal significant differences.

Fig. 9F shows that scale aspect ratio is different among regions on bluegill (ANOVA: $p = 0.033$). Tail scales have a lower aspect ratio than peduncle scales (Tukey HSD; tail–peduncle: $p = 0.045$). Lower aspect ratios indicate that scales are shorter in the dorsoventral axis or longer in the anteroposterior axis. Ventral and opercle scales have more variability in aspect ratio compared to other scales, as shown by the standard error bars in Fig. 9F.

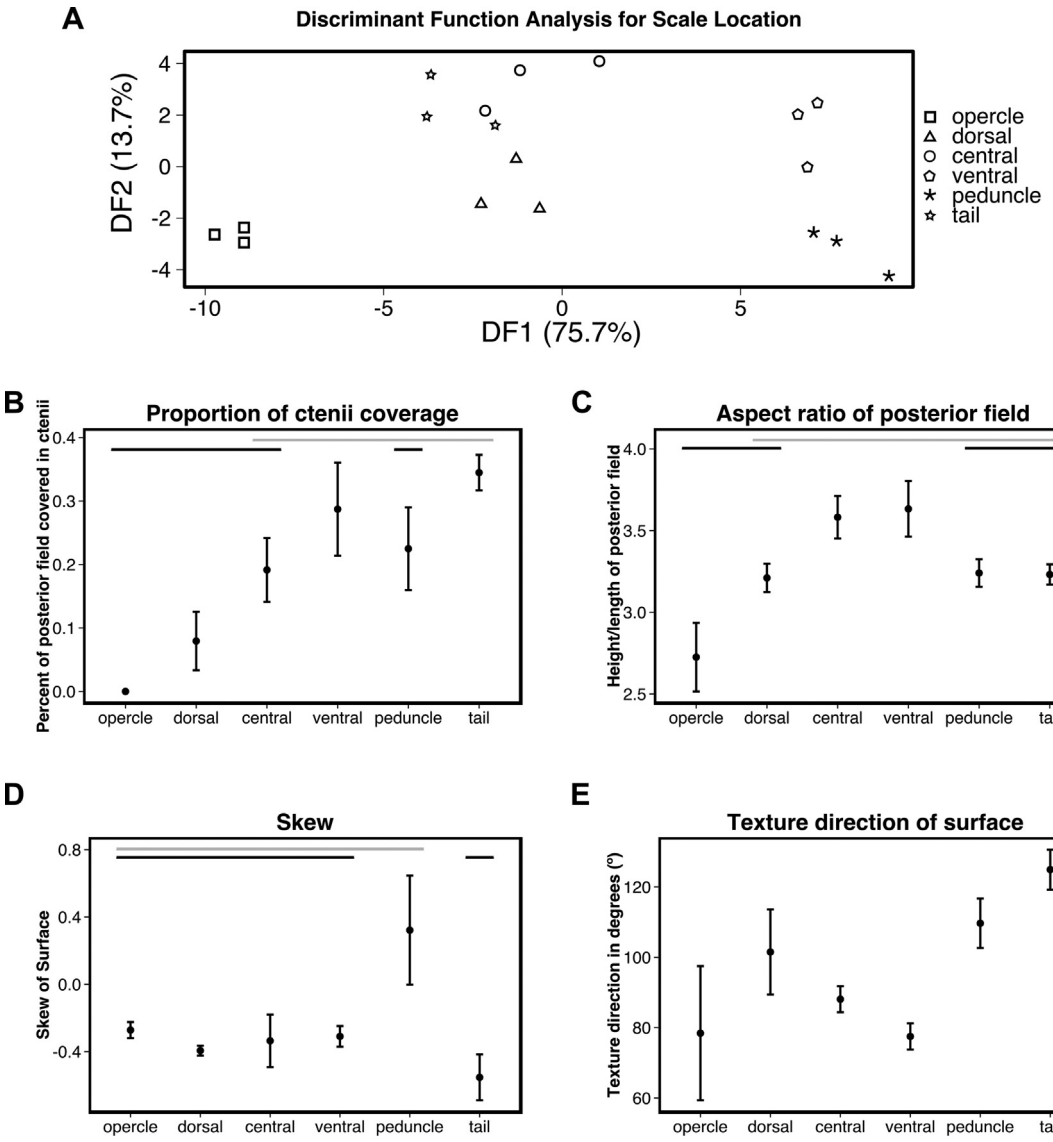

Fig. 8. Scale surface morphology data from GelSight, comparing measurements from different body regions. (A) Discriminant function analysis using 9 different variables categorized with scale location. Discriminant function 1 (DF1) accounts for 75.7% of the diversity among groups, while discriminant function 2 (DF2) accounts for 13.7%. Panels B–E show variables that demonstrate significant differences among scale locations. Black and grey bars at the top of graphs indicate the groups that are not statistically different using Tukey HSD test. Bars are ± 1 standard error and points are means. (B) Percent of the posterior scale field covered in ctenii. (C) Aspect ratio (height divided by length) of the posterior field within scales. (D) Skew and scale location. (E) Texture direction measured with respect to the y-axis, with clockwise turns in texture direction resulting in positive angle values. Although the ANOVA shows a significant effect with this variable, there are no differences among groups using Tukey HSD. Values are near 90 degrees, which is expected for horizontally arranged scales.

4. Discussion

In the present paper we present data on morphological differences among in situ patches and individual scales from six different regions of the body of bluegill sunfish. We collected our data using both a new surface analysis technique that allows 3D reconstruction of a fish's surface, and μCT to focus on the morphology of individual scales. We found numerous differences among regions of the body in both the shape and pattern of scales.

Fish scales have been the subject of research on topics ranging from species description (Jordan and Evermann, 1898; Miller, 1945) and analysis of age and growth (Everhart, 1950; Lane, 1954; Beardsley, 1967) to population discrimination (Barlow and Gregg, 1991; Margraf and Riley, 1993; Unwin and Lucas, 1993). Scales can be well preserved in the fossil record, and have been used to characterize species assemblages (Shackleton, 1987; McDowall and Lee, 2005), inform diet and food webs (Maisey, 1994), and describe extinct taxa (Goodrich, 1907; Zylberberg et al., 2010). Scale morphology has also been used to infer taxonomic relationships among fish taxa, starting notably with Louis Agassiz and his categorization of fish diversity based on scale morphology, but continuing to the present day (Agassiz, 1833; Goodrich, 1907; Kobayasi, 1955; Randall, 1955; Roberts, 1993; Kuusipalo, 1998; Lippitsch, 1998).

However, detailed descriptions of scale morphology and variation over the body have remained limited due to the lack of a method for imaging surface topography on patches of overlapping scales. Scanning electron micrographs and alizarin-stained scales provide clear images for 2D and linear morphometrics, but are not suitable for quantitative metrology and 3D analysis, or for examining the relationships among scales in situ on the body. Perhaps in part due to the general lack of quantitative imaging of fish scales, inferences about the hydrodynamic and locomotor function of scales have remained mostly indirect and speculative. Even basic questions such as "how rough is the surface of a fish?" and

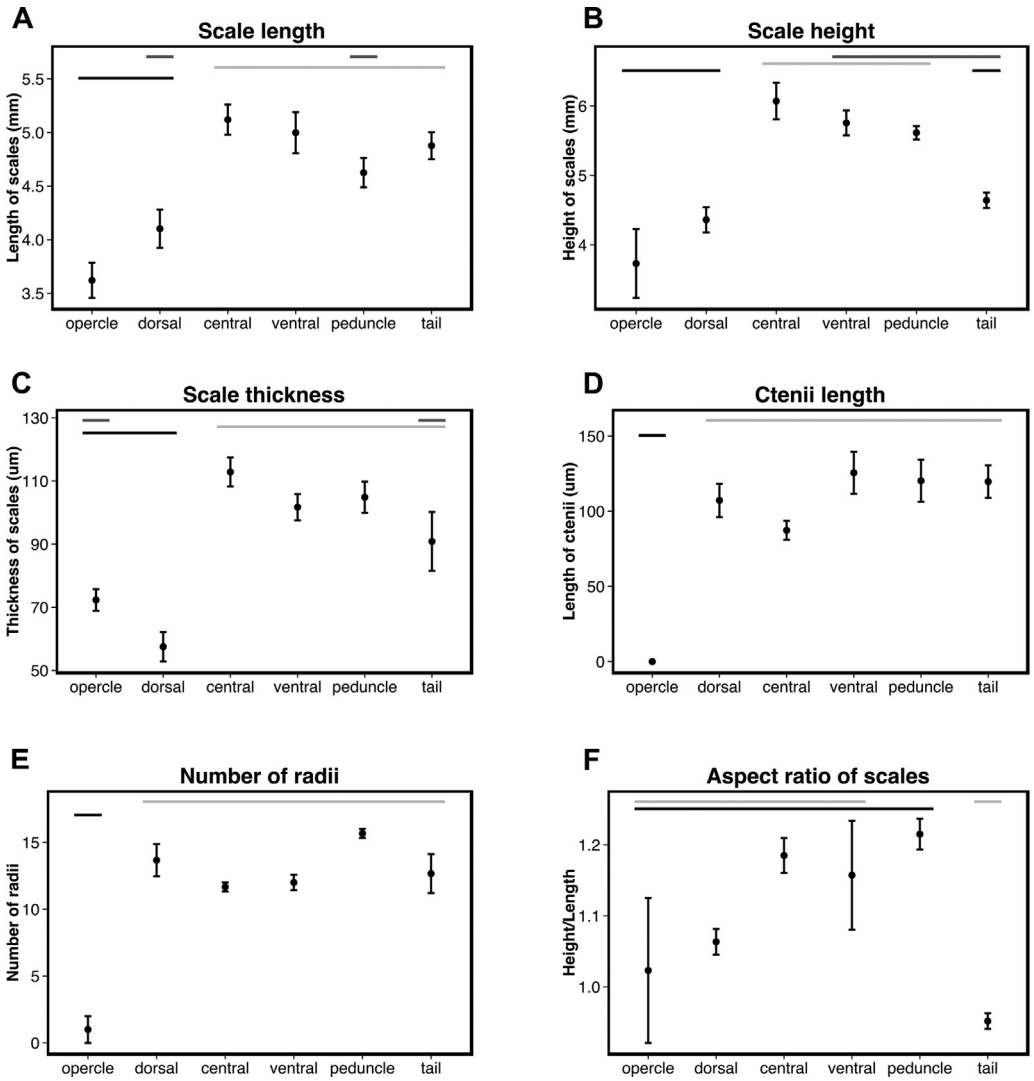

Fig. 9. Graphs of scale μCT data for scales all taken from the same individual to show differences in morphology among scales from different body regions. Lines at the top of graphs refer to groups determined with post-hoc Tukey HSD tests. Points are means and error bars are ± 1 standard error. (A) Scale length in the anterior-posterior direction. Scales from opercle and dorsal regions have the smallest lengths (3.5–4.3 mm) and bluegill scales show a range of lengths between 3.5–5.25 mm. (B) Scale height (dorsal–ventral direction). Scales from opercle, dorsal, and tail regions have the smallest heights, and variation of all scales is between 3 and 6.5 mm. (C) Scale thickness. Scales from dorsal and opercle regions are thinnest. Thickness ranges from 50 to 120 μm. (D) Ctenii length; all ctenii appear similar in length where present. Opercle scales have no ctenii. (E) Radii counts from different scale regions. Opercle scales have zero or few radii, while other scales have between 11 and 16. (F) Aspect ratio of whole scales. Scales are usually larger in height than length, except for scales on the tail and opercle regions.

"how does roughness vary across a fish's body surface?" have not been quantitatively addressed. Without this information, hypotheses about either how water flow is altered by scale morphology or regarding the effects of scales on boundary layer flows cannot be specified. To our knowledge, the present data on bluegill represent the first analysis of the 3D surface structure of scale patches and the use of μCT scans to investigate dimensional variation in individual scales around the body.

4.1. Bluegill scale morphology

Bluegill scales vary both qualitatively and quantitatively among different regions of the body. Figs. 2–7 illustrate scales from our six chosen regions. We particularly note the presence of ctenoid scales on all regions except the cycloid-scaled opercle, but differences do not end there.

Of our nine GelSight-measured variables for in situ scale patches, ctenii coverage, posterior field aspect ratio, skew, and texture direction show significant differences among different regions of the bluegill. In addition, μCT data on individual scales show differences in length, height, thickness, ctenii length, number of radii, and aspect ratio. Both the GelSight and μCT variables often show differences in the opercle, dorsal, peduncle, or tail regions compared to others, leading us to hypothesize that these regions may be good candidates for observing within-species scale diversity in other species. For example, to study differences in scale morphology within a species, scales from the opercle, dorsal, peduncle, and tail regions may be important to sample because these regions are most often different from other regions in the dataset we present here. Furthermore, because these regions appear to be most different, they may hold information on the functional significance of scale diversity – especially if similar patterns are seen in other species as some other studies suggest (Burdak, 1986; Grande and Bemis, 1998; Ibañez et al., 2009). Scales from the central and ventral regions are always very similar in our analyses and often have average values for metrics that we quantified; these may be good regions to use when investigating differences between species or describing the scales of a species.

Differences in the shape of the posterior fields are evident in our GelSight images of scale patches (panel B in Figs. 2–7). These differences are reflected in our analysis of posterior field aspect ratio (Fig. 8C) where we find the lowest aspect ratio on the opercle, followed by dorsal, peduncle, and tail regions, and then central and ventral regions. This aspect ratio pattern is mirrored in the analysis of whole scales (Fig. 9F) with a few differences. First, the aspect ratio of whole opercle scales has a much higher variability (Fig. 9F) than that of other regions, evidence that scale shape is more variable in the opercle than in other regions. Second, the aspect ratio of whole peduncle scales is high compared to that of other regions, but peduncle posterior fields have average aspect ratios. This last point is evidence that posterior field shape is not only the result of the shape of the whole scale; instead, scale shape interacts with the arrangement of neighboring scales to create different posterior field shapes. However, the general agreement between posterior field and whole scale aspect ratio patterns may indicate that whole scale shape often dictates posterior field shape, at least in bluegill.

In the order of largest to smallest, the largest scales in length, height, and thickness are the scales of the central, ventral, peduncle, and tail regions (Fig. 9A–C). Dorsal and opercle scales are overall smallest in those three simple size measurements. Ctenii length saw no pattern besides the lack of ctenii on opercle scales, although it is possible that slight differences exist, because central ctenii appear to be shorter than others (Fig. 9D). Radii show a pattern where opercle radii counts are different from those of other regions (Fig. 9F), yet radii counts appear to have small standard deviations in the central, ventral, and peduncle regions. Although we were unable to detect a significant difference between radii counts with our sample size, the pattern we describe here suggests a significant trend may emerge with further study and a larger sample size. Because radii are gaps in the ossification of scales, they naturally provide increased flexibility for scales. It is interesting to note that the highest radii counts come from regions of the body that are either naturally curved (dorsal) or experience higher lateral curvature during swimming (the caudal peduncle and tail). Because the opercular region does not bend during swimming, perhaps it is unsurprising that opercle scales have almost no radii, and hence, limited expected flexibility.

4.2. Functional significance of scale structures for solid mechanics

Research into the solid mechanics of fish scales has largely focused on biomimetic applications of fish-scale-like armor (Vernerey and Barthelat, 2010; Yang et al., 2012; Chintapalli et al., 2014). Much of this research has investigated thickened ganoid scales typical of Polypteridae and Lepisosteidae (Bruet et al., 2008; Song et al., 2011) but the mechanical properties of elasmoid scales as seen in bluegill and most bony fishes have also been investigated (Zhu et al., 2012; Browning et al., 2013). Here we present several hypotheses relevant to the solid mechanical function of fish scales based on the features that we have observed in bluegill scales.

First, the slight curvature of scales may function to stiffen scales in specific loading regimes. Scales appear to be curved so that their interior surfaces, facing medially, are concave (cross-sections in panel F of Figs. 2–7). This curvature would be expected to increase bending stiffness of the scale and allow it to resist bending in the anterior–posterior plane, which could be important in resisting injury or local deformation during swimming and escape events. Current mathematical and physical models of scales do not take scale curvature into account (Vernerey and Barthelat, 2010; Browning et al., 2013). Presumably scales contact and slide past one another during body and fin undulation (scales can be present on fins), but the degree and nature of scale-to-scale relative motion is unknown. It is also possible that scales could store elastic energy during either standard undulatory locomotion or high lateral bending maneuvers such as escape responses. Any elastic energy stored would be returned to the fish to accelerate lateral bending of the body in the opposite direction and scale curvature would affect the amount of energy stored. This hypothesis could be examined by first understanding the kinematics of fish scales during different modes of locomotion and then determining the extent of scale movement and bending in vivo.

Second, the circuli and other microroughness features on scale surfaces may function to limit tensile stresses to the valleys between circuli during bending of the scale (Yang et al., 2012). Limiting tensile stress in this way will minimize tensile stress during the bending of scales, which could affect the amount of stress necessary to produce a given amount of bending.

Third, circuli and other microroughness features of both scale medial and lateral surfaces could increase the second moment of area for scales. Increasing the second moment of area by placing material farther from the axis of bending would increase the stiffness of scales, with implications for swimming and protection as noted above.

Fourth, fields of interlocking ctenii at the posterior edge of scales may function as regions of flexibility. Because ctenii are made of many interlocking structures, it is reasonable to assume they are not as stiff as the body of the scale made of solid ossified tissue. The interlocking ctenii would create decreased resistance to flexibility, which could be important for lessening the force to bend arrays of scales when they are touching. This hypothesis is dependent upon the kinematics of scales during swimming and assumes that the posterior part of a scale will touch the scale posterior to it, creating a bending force.

A fifth hypothesis relevant to scale function is that radii may allow increased scale flexibility, thereby reducing body bending forces (Taylor, 1916) and the locomotor cost of transport. Radii are gaps in the ossified layer on scales, found on the anterior portion of scales on bluegill and other fishes (panel F in Figs. 3–7) (Daniels, 1996). Radii may decrease the bending stiffness of scales and these gaps could provide flexibility without sacrificing protective functions because radii are located under the surface of the neighboring scales in the anterior direction.

A final hypothesis on the solid mechanics of scales is that the microroughness of scales, including circuli and ctenii, could provide a substrate for the attachment of the epidermal and mucous layers atop fish scales. The epidermis and mucus could decrease friction among overlapping scales and make it easier for scales to slide past one another as the body bends, allowing for greater amounts of body curvature before scales begin to bend and resist body curvature. Interactions among biomimetic 3D-printed scales have been suggested to increase the cost of transport during locomotion, and scale mobility in sharks may act to decrease the energy required to bend the body (Wen et al., 2015).

4.3. Functional significance of scale structures for fluid mechanics

Scale morphology not only has relevance for solid mechanics and how fish body bending occurs, but for fluid mechanics as well. Several features of the pattern of scale variation across the body suggest functional hypotheses for future experimental testing. First, one hypothesis regarding scale function is that ctenoid scales increase turbulent energy in the boundary layer. This hypothesis originated in the Russian literature (Burdak, 1986), which states that spiny ctenoid scales create organized turbulence to either create or maintain a turbulent boundary layer, thereby delaying boundary layer separation and the associated increase in pressure drag. Although laminar boundary layers generate less friction drag than turbulent ones, turbulent boundary layers have a greater energy and are less prone to separation (Anderson et al., 2001; Anderson, 2005). If a fish were to ‘trip’ the boundary layer

from laminar to turbulent, it could therefore decrease drag by being less likely to incur separation – the spines on scales could be used as a turbulator (turbulence generator) in this manner. Our limited knowledge of swimming fish boundary layers shows that fish generate mainly laminar boundary layers (Anderson et al., 2001) at slow to moderate swimming speeds. However, turbulent boundary layers can occur posteriorly on the body and the tail, and during higher-amplitude motions such as escape responses. Also, larger fish may incur turbulent boundary layers proportionally further anteriorly on their bodies simply due to their large length – a factor in determining the Reynolds number and organization of boundary layer flows. For example, if the laminar-to-turbulent transition happens at 10 cm down the length of both a 15 cm salmon and a 60 cm salmon, the transition occurs proportionally further anteriorly on the 60 cm fish and we may expect the surface structure of the fish to reflect this. The hypothesis that ctenii increase turbulent energy in the boundary layer is often presented as if it was well supported (Bone and Moore, 2008; Helfman et al., 2009), but in fact we are not aware of any experimental studies that have investigated this idea explicitly.

Second, the increased ctenii coverage we observe towards the tail could indicate the use of more turbulators, such as ctenii, to delay separation of the boundary layer as the fluid's pressure gradient changes further back on the fish. We observed an increase in the coverage of ctenii as we move ventrally and posteriorly on the body (Fig. 8B), and as above, ctenii may be acting as turbulators to create a turbulent boundary layer and delay separation. In addition, it has been shown that both streamwise (parallel to the flow) riblets and the riblet-like features of shark's placoid scales reduce drag in turbulent boundary layers (Dean and Bhushan, 2010; Oeffner and Lauder, 2012; Wen et al., 2014) and the patterns of spines on fish scales could function similarly to reduce drag where there is turbulence. Furthermore, the increased ctenii coverage ventrally on the bluegill body might be explained by the increased turbulence created by pectoral fin oscillation during swimming at speeds of less than one body length per second (Gibb et al., 1994; Drucker and Lauder, 1999). In short, more ctenii are found where there appears to be increased turbulent flow, indicating that increasing the number the number of ctenii may be useful for controlling turbulence intensity near the body.

A related hypothesis for scale function is that the transition from cycloid scales on the anterior part of the body to ctenoid scales on the posterior part of the body could indicate the transition from a laminar to a turbulent boundary layer (Aleyev, 1977). Here, anterior cycloid scales would reduce drag in a laminar boundary layer by virtue of their smooth surface (Aleyev, 1977; Burdak, 1986). If the boundary layer becomes turbulent after the gill opening where fluid is injected into the boundary layer (Tytell and Alexander, 2007), then spiny-edged ctenoid scales could organize turbulence to prevent separation, as above. To test this hypothesis, experimental measurements of boundary layer flows could be made to determine if there is a match between where scales transition from cycloid to ctenoid and where the boundary layer transitions from laminar to turbulent flow.

Third, one of the surface metrology parameters measured from GelSight, skew, shows a pattern where the only positive values are seen on the peduncle region. Skew is a measurement of the dominance of peaks versus valleys on the surface, with positive values indicating more peaks. For reference, most sandpapers have skew values from 0.7 to 1.0 (a flat surface with grains that create peaks) and our data shows skew values of about 0.4 for the peduncle, indicating dominance of peaks. The peduncle of fish experiences larger amounts of bending than other regions, and the flow speed of the fluid near the peduncle is increased due to higher body oscillation amplitudes. In addition, the peduncle is a region of complex three-dimensional flow (Nauen and Lauder, 2001). Perhaps the positive skew values in the peduncle region have some relationship to the complex and possibly separated flows in this region (Anderson et al., 2001).

Although there has been discussion about the role of ctenii in hydrodynamics (see above), it is possible that the circuli may also function as turbulators. Circuli are concentric growth rings on the body of scales that protrude a small amount (~5 μm in bluegill) from the scale surface. On the dorsal and ventral areas of each scale, these circuli have streamwise grooves, while the posterior parts of scales have circuli perpendicular to flow. Circuli could generate turbulence to create or maintain a turbulent boundary layer. Circuli could also concentrate fluid shear stress on their ridges while experiencing a drop in shear stress over valleys, with the effect of decreasing friction drag overall.

Finally, the epidermis and mucus that cover the body and scales of many fish may have a profound effect on scale function. It is possible that the mucus layer and epidermis of live fish covers or partially obscures some of the morphological features described above. Values for thickness of the epidermis for trout and salmon vary from about 30 μm to 90 μm (Fast et al., 2002), which if similar in bluegill, may obscure microroughness created by circuli. Ctenii appear to project through the epidermis and mucus coating, as they are visible in experimental GelSight imaging of the surface of live bluegill swimming (D.K.W., unpublished observations). However, the epidermis may also conform to the scale surface, allowing many of the larger features to affect the fluid moving past the body.

Our study used preserved specimens but the epidermis is still sometimes present as a smooth area with small 10 μm bumps (perhaps goblet cells) in the anterior part of posterior fields of the images shown (Figs. 2B and 7B). However, the epidermis is likely distorted and damaged by the preservation process and live fish may look quite different. Mucus is almost certainly not present in our images, as the fixation and preservation process often causes mucus to slough off. If the epidermis and mucus of fish normally cover features such as circuli and ctenii, then these structures are not likely to have a direct effect on the boundary layer of a swimming fish, thereby limiting the fluid dynamic effect of several scale features. In fact, circuli and fields of ctenii may have a role in retaining the mucus coat on the scale surface.

Despite this range of hypotheses concerning scale function, the nature of fluid flow at the level of fish scales remains unknown, and so the effect of scale microstructure on flow dynamics over the body of swimming fishes is an area very much in need of future study.

4.4. The future of 3D fish scale imaging

With the use of both established μCT techniques and the new 3D surface imaging provided by GelSight, we have shown that it is possible to collect quantitative data on fish scale morphology. Describing scale morphology in 3D is crucial to understanding any potential hydrodynamic interactions scales may be having with the external fluid, and such data may also shed light onto other functional roles for scales. The scales of more species could be studied with these techniques to measure patterns of scale morphology in a phylogenetic context, which may lead to further hypotheses about the functional roles of scale 3D structure. Furthermore, it would be interesting to see if the general patterns across the body that we observed in bluegill hold in other species. GelSight is a powerful imaging tool that can be used to study scales from fossil fish to the surfaces of live fish. Additionally, 3D shape data allows us to create physical models of fish surfaces using 3D printing techniques and then test their performance during both swimming and static tests (Wen et al., 2014, 2015). In this way we can link form to function by testing the mechanical and hydrodynamic performance of different

scale structures using physical models and imaging the surface of live fish during locomotion.

Acknowledgements

This work was supported by ONR MURI Grant N000141410533 monitored by Dr. Bob Brizzolara and NSF GRF 2014162421 awarded to D.K.W. The authors thank Bill Yost and Kimo Johnson of GelSight for their assistance with the GelSight imaging technique, and Karsten Hartel and Andy Williston of the Harvard MCZ Fish Department for their assistance and suggestions. Special thanks to James Weaver for his assistance with this project and for introducing us to GelSight. Many thanks also to Stacy Farina and Kelsey Lucas for their helpful comments on the manuscript.

References

Agassiz, L., 1833. Recherches sur les Poissons Fossiles, vol. 2. Imp. Petitpierre, Neuchatel.
Aleyev, Y.G., 1977. In: Junk, W. (Ed.), Nekton. The Hague.
Anderson, E.J., McGillis, W.R., Grosenbaugh, M.A., 2001. The boundary layer of swimming fish. J. Exp. Biol. 204, 81–102.
Anderson, J.D., 2005. Ludwig Prandtl's boundary layer. Phys. Today 58, 42–48.
Barlow, C.G., Gregg, B.A., 1991. Use of circuli spacing on scales to discriminate hatchery and wild barramundi: *Lates calcarifer* (Bloch). Aquac. Fish. Manag. 22, 491–498.
Batts, B.S., 1964. Lepidology of the adult pleuronectiform fishes of Puget Sound Washington. Copeia 1964, 666–673.
Beardsley, G.L., 1967. Age, growth, and reproduction of the dolphin, *Coryphaena hippurus*, in the Straits of Florida. Copeia 1967, 441–451.
Bone, Q., Moore, R.H., 2008. Biology of Fishes, 3rd ed. Taylor and Francis, New York.
Browning, A., Ortiz, C., Boyce, M.C., 2013. Mechanics of composite elasmoid fish scale assemblies and their bioinspired analogues. J. Mech. Behav. Biomed. Mater. 19, 75–86.
Bruet, B.J.F., Song, J., Boyce, M.C., Ortiz, C., 2008. Materials design principles of ancient fish armour. Nat. Mater. 7, 748–756.
Burdak, V.D., 1986. Morphologie fonctionnelle du tegument ecailleux des poissons. Cybium 10, 1–128.
Chintapalli, R.K., Mirkhalaf, M., Dastjerdi, A.K., Barthelat, F., 2014. Fabrication, testing and modeling of a new flexible armor inspired from natural fish scales and osteoderms. Bioinspir. Biomim. 9, 036005.
Cockerell, T.D.A., 1911. The scales of freshwater fishes. Biol. Bull. 20, 367–387.
Daniels, R.A., 1996. Guide to the identification of scales of inland fishes of northeastern North America. New York State Mus. Bull. 488, 1–93.
Dapar, M.L.G., Torres, M.A.J., Fabricante, P.K., Demayo, C.G., 2012. Scale morphology of the Indian goatfish, *Parapeneus indicus* (Shaw, 1803) (Perciformes: Mullidae). Adv. Environ. Biol. 6, 1426–1432.
Dean, B., Bhushan, B., 2010. Shark-skin surfaces for fluid-drag reduction in turbulent flow: a review. Phil. Trans. R. Soc. A 368, 4775–4806.
Drucker, E.G., Lauder, G.V., 1999. Locomotor forces on a swimming fish: three-dimensional vortex wake dynamics quantified using digital particle image velocimetry. J. Exp. Biol. 202, 2393–2412.
Drucker, E.G., Lauder, G.V., 2000. A hydrodynamic analysis of fish swimming speed: wake structure and locomotor force in slow and fast labriform swimmers. J. Exp. Biol. 203, 2379–2393.
Ellerby, D.J., Gerry, S.P., 2011. Sympatric divergence and performance trade-offs of bluegill ecomorphs. Evol. Biol 38, 422–433.
Esmaeili, H.R., Ansari, T.H., Teimory, A., 2007. Scale structure of a cyprinid fish *Capoeta damascina* (Valenciennes in Cuvier and Valenciennes, 1842) using scanning electron microscope (SEM). Iran. J. Sci. Technol. Trans. A. 31, 255–262.
Everhart, W.H., 1950. A critical study of the relation between body length and several scale measurements in the smallmouth bass, *Micropterus dolomieu* Lacepede. J. Wildl. Managem. 14, 266–276.
Fast, M.D., Sims, D.E., Burka, J.F., Mustafa, A., Ross, N.W., 2002. Skin morphology and humoral non-specific defence parameters of mucus and plasma in rainbow trout, coho and Atlantic salmon. Comp. Biochem. Physiol. Part A Mol. Integr. Physiol. 132, 645–657.
Flammang, B.E., Lauder, G.V., 2008. Speed-dependent intrinsic caudal fin muscle recruitment during steady swimming in bluegill sunfish, *Lepomis macrochirus*. J. Exp. Biol. 211, 587–598.
Flammang, B.E., Lauder, G.V., Troolin, D.R., Strand, T.E., 2011. Volumetric imaging of fish locomotion. Biol. Lett. 7, 695–698.
Gerry, S.P., Wang, J., Ellerby, D.J., 2011. A new approach to quantifying morphological variation in bluegill *Lepomis macrochirus*. J. Fish Biol. 78, 1023–1034.
Gibb, A.C., Jayne, B.C., Lauder, G.V., 1994. Kinematics of pectoral fin locomotion in the bluegill sunfish *Lepomis macrochirus*. J. Exp. Biol. 189, 133–161.
Goodrich, E.S., 1907. On the scales of fish, living and extinct, and their importance in classification. Proc. Zool. Soc. 1907, 751–773.
Grande, L., Bemis, W.E., 1998. A comprehensive phylogenetic study of amiid fishes (Amiidae) based on comparative skeletal anatomy. An empirical search for interconnected patterns of natural history. J. Vertebr. Paleontol., Spec. Mem. 4 (Suppl. to Vol. 18).
Helfman, G.S., Collette, B.B., Facey, D.E., Bowen, B.W., 2009. The Diversity of Fishes, 2nd ed. John Wiley and Sons, Hoboken, NJ.
Ibañez, A.L., Cowx, I.G., OHiggins, P., 2009. Variation in elasmoid fish scale patterns is informative with regard to taxon and swimming mode. Zool. J. Linn. Soc. 155, 834–844.
Jawad, L.A., 2005. Comparative scale morphology and squamation patterns in triplefins (Pisces: Teleostei: Perciformes: Tripterygiidae). Tuhinga 16, 137–167.
Jayne, B.C., Lozada, A.F., Lauder, G.V., 1996. Function of the dorsal fin in bluegill sunfish: motor patterns during four distinct locomotor behaviors. J. Morphol. 228, 307–326.
Johnson, M.K., Adelson, E.H., 2009. Retrographic sensing for the measurement of surface texture and shape. Proceedings of the IEEE Conference on Computer Vision and Pattern Recognition, pp. 1070–1077, http://dx.doi.org/10.1109/CVPR.2009.5206534.
Johnson, M.K., Cole, F., Raj, A., Adelson, E.H., 2011. Microgeometry capture using an elastomeric sensor. Proceedings of ACM SIGGRAPH, http://dx.doi.org/10.1145/1964921.1964941 (article no. 46).
Jordan, D.S., Evermann, B.W., 1898. The fishes of North and Middle America: a descriptive catalogue of the species of fish-like vertebrates found in the waters of North America, north of the Isthmus of Panama. Part 2. Bull. U.S. Nat. Mus. 47, 1241–2183.
Kendall, J.L., Lucey, K.S., Jones, E.A., Wang, J., Ellerby, D.J., 2007. Mechanical and energetic factors underlying gait transitions in bluegill sunfish (*Lepomis macrochirus*). J. Exp. Biol. 210, 4265–4271.
Kobayasi, H., 1955. Comparative studies of the scales in Japanese freshwater fishes, with special reference to phylogeny and evolution. IV. Particular lepidology of freshwater fishes. I. Suborder Isospondyli (continued). Jap. J. Ichthyol. IV, 64–75.
Kuusipalo, L.V., 1998. Scale morphology in Malawian cichlids. J. Fish Biol. 52, 771–781.
Lagler, K.F., 1947. Lepidological studies, 1. Scale characters of the families of Great Lakes fishes. Trans. Am. Microsc. Soc. 66, 149–171.
Lane, C.E., 1954. Age and growth of the bluegill, *Lepomis macrochirus* (Rafinesque), in a new Missouri impoundment. J. Wildl. Manag. 18, 358–365.
Li, R., Adelson, E.H., 2013. Sensing and recognizing surface textures using a GelSight sensor. Proceedings of the IEEE Conference on Computer Vision and Pattern Recognition, pp. 1241–1247, http://dx.doi.org/10.1109/CVPR.2013.164.
Li, R., Platt, R.J., Wenzhen, Y., Pas, A., Roscup, N., Srinivasan, M.A., Adelson, E., 2014. Localization and manipulation of small parts using GelSight tactile sensing. Proceedings of the IEEE International Conference on intelligent Robots and Systems, pp. 3988–3993 http://dx.doi.org/10.1109/IROS.2014.6943123.
Lippitsch, E., 1998. Phylogenetic study of cichlid fishes in Lake Tanganyika: a lepidological approach. J. Fish Biol. 53, 752–766.
Maisey, J.G., 1994. Predator–prey relationships and trophic level reconstruction in a fossil fish community. Environ. Biol. Fishes 40, 1–22.
Margraf, F.J., Riley, L.M., 1993. Evaluation of scale shape for identifying spawning stocks of coastal Atlantic striped bass (*Morone saxatilis*). Fish. Res. 18, 163–172.
McDowall, R.M., Lee, D.E., 2005. Probable perciform fish scales from a Miocene freshwater lake deposit Central Otago New Zealand. J. R. Soc. New Zeal. 35, 339–344.
Miller, R.R., 1945. A new cyprinid fish from Southern Arizona, and Sonora, Mexico, with the description of a new subgenus of *Gila* and a review of related species. Copeia 1945, 104–110.
Nauen, J.C., Lauder, G.V., 2001. Locomotion in scombrid fishes: visualization of flow around the caudal peduncle and finlets of the chub mackerel *Scomber japonicus*. J. Exp. Biol. 204, 2251–2263.
Oeffner, J., Lauder, G.V., 2012. The hydrodynamic function of shark skin and two biomimetic applications. J. Exp. Biol. 215, 785–795.
Randall, J.E., 1955. An analysis of the genera of surgeon fishes (family Acanthuridae). Pacific Sci. 9, 359–367.
Rasband, W.S., 1997–2015. ImageJ. U. S. National Institutes of Health, Bethesda, MD, USA http://imagej.nih.gov/ij/.
Richards, R.A., Esteves, C., 1997. Use of scale morphology for discriminating wild stocks of Atlantic striped bass. Trans. Am. Fish. Soc. 126, 919–925.
Roberts, C.D., 1993. Comparative morphology of spined scales and their phylogenetic significance in the Teleostei. Bull. Mar. Sci. 52, 60–113.
Sagong, W., Kim, C., Choi, S., Jeon, W.-P., Choi, H., 2008. Does the sailfish skin reduce the skin friction like the shark skin? Phys. Fluids 20, 110150.
Shackleton, L.Y., 1987. A comparative study of fossil fish scales from three upwelling regions. South African J. Mar. Sci. 5, 79–84.
Sire, J.-Y., Akimenko, M.-A., 2004. Scale development in fish: a review, with description of sonic hedgehog (shh) expression in the zebrafish (*Danio rerio*). Int. J. Dev. Biol. 48, 233–247.
Song, J., Ortiz, C., Boyce, M.C., 2011. Threat-protection mechanics of an armored fish. J. Mech. Behav. Biomed. Mater. 4, 699–712.
Standen, E.M., Lauder, G.V., 2005. Dorsal and anal fin function in bluegill sunfish *Lepomis macrochirus*: three-dimensional kinematics during propulsion and maneuvering. J. Exp. Biol. 208, 2753–2763.
Sudo, S., Tsuyuki, K., Ito, Y., Ikohagi, T., 2002. A study on the surface shape of fish scales. Jap. Soc. Mech. Eng. 45, 1100–1105.
Suzuki, T., 1971. Some scale patterns of the scad *Decapterus maruadsi* (Temminck et Schlegel), and their variations with body parts. Bull. Jap. Sea Reg. Fish. Res. Lab. 23, 1–19.

Taylor, H.F., 1916. The structure and growth of the scales of the squeteague and the pigfish as indicative of life history. Bull. U.S. Bur. Fish. 34, 285–330.
Tytell, E.D., Alexander, J.K., 2007. Bluegill *Lepomis macrochirus* synchronize pectoral fin motion and opercular pumping. J. Fish Biol. 70, 1268–1279.
Unwin, M.J., Lucas, D.H., 1993. Scale characteristics of wild and hatchery chinook salmon (*Oncorhynchus tshawytscha*) in the Rakaia River. New Zealand, and their use in stock identification. Can. J. Fish. Aquat. Sci. 50, 2475–2484.
Vernerey, F.J., Barthelat, F., 2010. On the mechanics of fishscale structures. Int. J. Solids Struct. 47, 2268–2275.
Wen, L., Weaver, J.C., Lauder, G.V., 2014. Biomimetic shark skin: design, fabrication and hydrodynamic function. J. Exp. Biol. 217, 1656–1666.
Wen, L., Weaver, J.C., Thornycroft, P.J.M., Lauder, G.V., 2015. Hydrodynamic function of biomimetic shark skin: effect of denticle pattern and spacing. Bioinspir. Biomim. 10, 066010 http://dx.doi.org/10.1088/1748-3190/10/6/066010.
Whitehouse, D.J., 1994. Handbook of Surface Metrology. Institute of Physics Publishing, Philadelphia.
Yang, W., Chen, I.H., Mckittrick, J., Meyers, M.A., 2012. Flexible dermal armor in nature. JOM 64, 475–485.
Zhu, D., Ortega, C.F., Motamedi, R., Szewciw, L., Vernerey, F., Barthelat, F., 2012. Structure and mechanical performance of a modern fish scale. Adv. Eng. Mater. 14, 185–194.
Zylberberg, L., Meunier, F.J., Laurin, M., 2010. A microanatomical and histological study of the postcranial dermal skeleton in the Devonian sarcopterygian *Eusthenopteron foordi*. Acta Palaeontol. Pol. 55, 459–470.